



Response of real-time black carbon mass instruments to mini-CAST soot

Lukas Durdina, Prem Lobo, Max B. Trueblood, Elizabeth A. Black, Steven Achterberg, Donald E. Hagen, Benjamin T. Brem & Jing Wang

To cite this article: Lukas Durdina, Prem Lobo, Max B. Trueblood, Elizabeth A. Black, Steven Achterberg, Donald E. Hagen, Benjamin T. Brem & Jing Wang (2016) Response of real-time black carbon mass instruments to mini-CAST soot, *Aerosol Science and Technology*, 50:9, 906-918, DOI: [10.1080/02786826.2016.1204423](https://doi.org/10.1080/02786826.2016.1204423)

To link to this article: <https://doi.org/10.1080/02786826.2016.1204423>

 View supplementary material 

 Published online: 22 Jun 2016.

 Submit your article to this journal 

 Article views: 2048

 View related articles 

 View Crossmark data 

 Citing articles: 16 View citing articles 



Response of real-time black carbon mass instruments to mini-CAST soot

Lukas Durdina^{a,b}, Prem Lobo^c, Max B. Trueblood^c, Elizabeth A. Black^c, Steven Achterberg^c, Donald E. Hagen^c, Benjamin T. Brem^{a,b}, and Jing Wang^{a,b}

^aLaboratory of Advanced Analytical Technologies, Empa, Dübendorf, Switzerland; ^bInstitute of Environmental Engineering (IfU), ETH Zürich, Zürich, Switzerland; ^cCenter of Excellence for Aerospace Particulate Emissions Reduction Research, Missouri University of Science and Technology, Rolla, Missouri, USA

ABSTRACT

Soot is a climate forcer and a dangerous air pollutant that has been increasingly regulated. In aviation, regulatory measurements of soot mass concentration in the exhaust of aircraft turbine engines are to be based on measurements of black carbon (BC) calibrated to elemental carbon (EC) content of diffusion flame soot. The calibration soot must currently meet only one criterion: minimum EC to total carbon (TC) ratio of 0.8. However, not including soot properties other than the EC/TC ratio may potentially lead to discrepancies between different BC measurements. We studied the response of two instruments, the AVL Micro-Soot Sensor (MSS) and the Artium Laser-Induced Incandescence 300 (LII), to soot from two miniature combustion aerosol standard (mini-CAST) burners. By changing the air-fuel ratio, premixing nitrogen into the fuel, and using a catalytic stripper to remove volatile compounds, we produced a wide range of particle morphologies and EC contents. As the EC content decreased, both the instruments underreported the EC mass, but the LII diverged more severely. Upon closer investigation of eight conditions with EC/TC > 0.8, the LII underreporting was found independent of primary particle size, but increased with decreasing geometric mean diameter of the soot agglomerates. As the geometric mean diameter decreased from 160 nm to 50 nm, the differences between the LII and MSS increased from 15% to 50%. The results suggest that in addition to EC content, calibration procedures for the regulatory BC measurements may need to take particle size distributions into account.

ARTICLE HISTORY

Received 27 November 2015
Accepted 10 June 2016

EDITOR

Matti Maricq

1. Introduction

Incomplete combustion of hydrocarbon fuels produces soot, a toxic air pollutant, and a climate forcer. Soot has been increasingly studied because it impacts radiative fluxes (Jacobson 2001; Menon et al. 2002; Ramanathan and Carmichael 2008; Bond et al. 2013) and increases susceptibility to allergies and lung, heart, and nervous system diseases (Oberdorster et al. 2004; Attfield et al. 2012; Ristovski et al. 2012; Ostro et al. 2015). The mounting evidence of adverse impacts of soot has led to increasingly more stringent regulations of particulate matter (PM) emissions. For example, new diesel and direct injection gasoline engines in Europe must comply with PM mass and number concentration limits (DieselNet 2016). Exhaust soot concentrations have been substantially reduced due to advances in exhaust aftertreatment and combustion systems, which has introduced new demands for instruments sensitive and specific

only to the quantity regulated. For measurements of soot mass concentration, researchers have evaluated real-time instruments based on aerosol optical absorption: photoacoustic, interferometric, incandescence, and filter-based methods (Mohr et al. 2005; Sheridan et al. 2005; Cross et al. 2010; Giechaskiel et al. 2014; Lobo et al. 2015). Light absorption instruments need to be calibrated to report mass concentration. However, reported mass concentrations can differ by more than 15% when the soot measured differs significantly from the calibration material as well as due to interference and sensitivity to exhaust components other than soot (Saathoff et al. 2003; Giechaskiel et al. 2014). Since there has not been a universal standard reference material for soot (Baumgardner et al. 2012), emission standards need to devise soot definitions and calibration procedures ensuring that various compliant instruments perform similarly

CONTACT Lukas Durdina ✉ Lukas.Durdina@empa.ch 📧 Laboratory of Advanced Analytical Technologies, Empa, Überlandstrasse 129, Dübendorf, CH-8600, Switzerland; Prem Lobo ✉ plobo@mst.edu 📧 Center of Excellence for Aerospace Particulate Emissions Reduction Research, Missouri University of Science and Technology, Rolla, MO 65409, USA; Jing Wang ✉ jing.wang@ifu.baug.ethz.ch 📧 Institute of Environmental Engineering (IfU), ETH Zürich, Zürich, Switzerland.
Color versions of one or more of the figures in the article can be found online at www.tandfonline.com/uast.

📎 Supplemental data for this article can be accessed on the [publisher's website](#).

on the calibration aerosol and the soot source for which they are intended.

Real-time optical soot instruments will be used for regulatory measurements of non-volatile PM (nvPM) emissions from aircraft turbine engines. NvPM is defined as particles sampled at the engine exit plane that remain solid when heated to 350°C (SAE 2013). The regulation will require measurement of both nvPM number and mass concentrations. Total nvPM mass concentration can be directly measured only by filter sampling and analysis, which can be time consuming, costly, and affected by measurement artifacts (Subramanian et al. 2007; Lack et al. 2008). Therefore, the regulatory standard considers the most appropriate method for representing the nvPM mass concentration to be the online measurement of black carbon (BC) mass concentration.

Compliant instruments measuring BC mass concentration are to be calibrated to the mass of elemental carbon (EC) determined by thermal-optical analysis, currently the most applicable method (SAE 2013). The method is originally based on National Institute of Occupational Safety and Health (NIOSH) Method 5040 for diesel particulate matter (Birch and Cary 1996; NIOSH 2003). BC is defined based on optical properties as a soot fraction that strongly absorbs visible light, whereas EC is defined based on thermochemical properties as a refractory carbon that can be removed from a filter under an oxidizing carrier gas (NIOSH 2003). Both BC and EC are defined as the difference between the total carbon (TC) and organic carbon (OC), but OC has different definitions based both on optical properties (non-absorbing), and thermochemical properties (non-refractory) that may not be equivalent. In terms of molecular structures, BC and EC both represent the graphite-like material in soot, but the boundaries between BC and OC, and EC and OC only depend on the methods applied (Pöschl 2005). For aircraft turbine engine soot, BC and EC are considered almost equivalent (Petzold et al. 2011).

Currently, two real-time BC instruments comply with the specifications for standardized measurement of nvPM mass-based emissions from aircraft turbine engines (SAE 2013): the Micro-Soot Sensor (MSS; AVL LIST GmbH, Graz, Austria) and the laser-induced incandescence instrument LII 300 (LII; Artium Technologies Inc., Sunnyvale, CA, USA). To differentiate between the BC mass concentrations reported by these instruments, we use the terminology of Lack et al. (2014) and Petzold et al. (2013). The MSS measures the mass concentration of the equivalent BC (eBC), which is BC derived from optical absorption measurement. The LII measures the mass concentration of the refractory BC (rBC), which is the BC derived from incandescence methods. Hereafter we use the terms rBC, eBC, BC, nvPM, EC, and OC

when we refer to mass concentrations, if not stated otherwise. The MSS and LII output signals are directly proportional to EC content of combustion engine soot (Mohr et al. 2005). To measure nvPM mass concentrations in the aircraft turbine engine exhaust, the instruments must be calibrated to EC mass of diffusion flame soot containing $\geq 80\%$ EC. Such calibrated instruments must also demonstrate that they agree with EC mass concentration within $\pm 16\%$ on turbine engine exhaust (SAE 2013).

Since it is impractical and costly to use turbine engines for periodic calibrations, nvPM mass instruments have been calibrated with gas-fueled soot generators. A popular laboratory burner used is the miniature combustion aerosol standard (mini-CAST; Jing, Ltd., Zollikofen, Switzerland). Mini-CAST soot properties, such as mean agglomerate size, morphology, and EC concentrations, can be varied over a wide range by changing the air-fuel ratio and diluting the fuel with nitrogen (Moore et al. 2014). While the burner settings for generating soot with the highest EC content vary for the different models, for any mini-CAST, EC content decreases with decreasing mean agglomerate size (Crayford et al. 2013; Maricq 2014; Moore et al. 2014; Kim et al. 2015). Mini-CAST conditions that produce the largest particles (geometric mean diameter of the agglomerates, d_g , typically > 100 nm) have been found to well match the BC content of engine exhaust soot (Maricq 2014).

Aircraft turbine engine soot has unique characteristics potentially irreproducible by soot generators: small agglomerate size ($d_g < 50$ nm) and EC content of up to 90%. For a typical turbofan engine, d_g , effective density, and EC content increase with engine power (Agrawal et al. 2008; Petzold et al. 2011; Durdina et al. 2014; Lobo et al. 2015). To mimic aircraft turbine engine soot, previous studies either used diffusion flame soot with similar particle size distributions (Liscinsky et al. 2013; Stettler et al. 2013; Wong et al. 2013), or, for the development of the aircraft turbine engine nvPM standard, used EC-rich soot without considering other properties (Lobo et al. 2015). Since the EC content is the only requirement for the calibration aerosol, it is unclear to what extent the eBC and rBC are equivalent to EC over a wide range of particle composition and morphologies. During inter-comparison tests on various in-service aircraft turbine engines in 2012, the MSS and LII overall agreed within 15%, but then the instruments were not yet fully compliant with the standard calibration protocol (Lobo et al. 2015). In a follow-up study in 2013, with the MSS and LII calibrated in parallel, the LII reported on average 30% lower nvPM mass concentrations (Durdina et al. 2014). It was hypothesized that these differences could be attributed to different morphology of the calibration

aerosol and gas turbine soot that were affecting the instruments response.

Here, we investigate the response of the MSS and LII to mini-CAST soot with a wide range of EC contents and morphologies. We used two mini-CAST burners, models 5201C and 6203C, to produce 28 test conditions from fuel-rich to fuel-lean. We first look at the overall correlation of the rBC and eBC to EC as a function of the EC/TC ratio. Then we focus on eight settings, four for each burner, which met the sole calibration soot criterion of $EC/TC \geq 80\%$. For these conditions, we look at the potential effects of particle effective density, geometric mean agglomerate size, and primary particle size on the instrument response. This work has implications for the development of the nvPM emissions measurement protocol for aircraft turbine engines and in a broader sense for future PM regulations of other sources, such as marine engines (Lack and Corbett 2012), which might adopt a similar methodology.

2. Methods

2.1. Mini-CAST operating conditions and sample conditioning

The mini-CAST consists of a co-flow diffusion flame propane burner, and a quench and dilution track (Figure 1). In the quench track, nitrogen dilutes the particle stream, stops the combustion processes, and inhibits water condensation at room temperature. The quenched sample is then further diluted with air (we used dried and filtered compressed air). The fuel can be diluted with nitrogen (referred to here as N_2 premix), which offers additional settings to modify the particle properties and composition. The user can control the fuel (Q_f), oxidation air (Q_a), N_2 premix ($Q_{mix N_2}$), and dilution air (Q_{dil}) flows, whereas the quench N_2 (Q_{N_2}) is typically fixed. The two mini-CAST models 5201C and 6203C used in this study

differ in geometry, flows, and soot mass output. The 6203C contains a smaller burner with the quench track located closer to the burner than in the 5201C, which results in formation of smaller agglomerates (Jing 2002) and up to factor 20 lower soot mass than the 5201C.

We produced 28 test conditions by varying the air-fuel mixture, N_2 premix, and sample treatment by a catalytic stripper (CS; Catalytic Instruments GmbH, Rose-heim, Germany) to remove OC (summary of the test conditions can be found in Table S1 in the online supplementary information, SI). To characterize the flame conditions at each test point, we used the global fuel-air equivalence ratio ϕ and atomic carbon/oxygen ratio (C:O). ϕ is the actual fuel-air mass flow ratio divided by the stoichiometric fuel-air ratio (0.0641 for propane, by weight). Thus, the mixture is rich if $\phi > 1$, lean if $\phi < 1$, and stoichiometric if $\phi = 1$. ϕ and C:O are linearly dependent. C:O was calculated from the fuel and air densities, and C and O atomic weights and fractions in the fuel and air, respectively, resulting in the equation: $7.316 \times Q_f/Q_a$, where Q_f and Q_a are the fuel and oxidation air flow rates, respectively (2.2% difference from Schnaiter et al. (2006) that used $7.16 \times Q_f/Q_a$). The C:O and ϕ conditions investigated in this study spanned flame conditions from fuel-rich (5201C) to fuel-lean (6203C) with overlapping settings between the two mini-CASTs. These parameters facilitate comparison between different burners, but they ignore the N_2 premix and quench flow rates, as well as the different burner geometries, thus the same ϕ and C:O may generate soot with different characteristics (see the SI).

Mini-CAST exhaust was diluted in several stages to accommodate the optimal measurement range of various instruments. Since the mini-CAST 5201C generated considerably higher soot concentration, its exhaust was first passed through a multi-stage HEPA filter dilution bridge (dilution factor typically set to ~ 20). All the sample lines were kept at room temperature because the internal

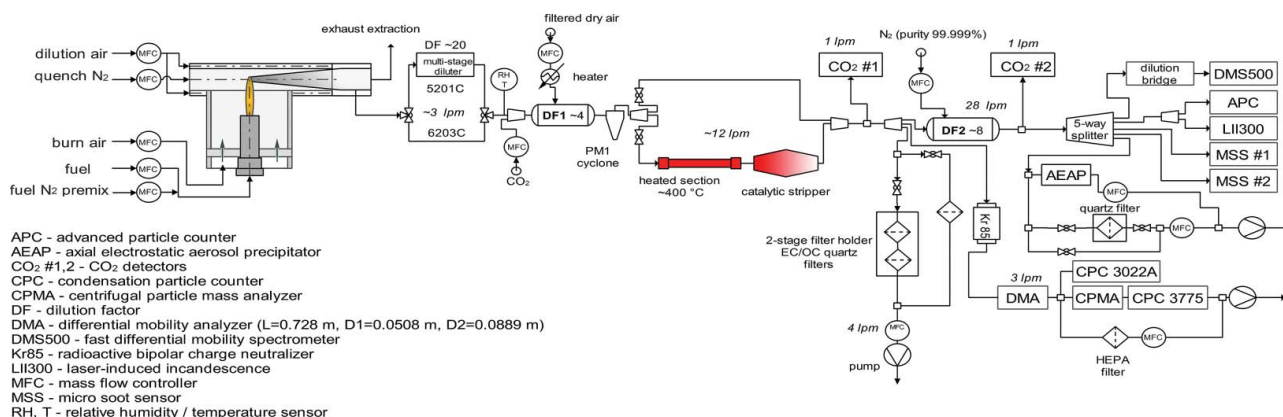


Figure 1. Experimental setup.

dilution of the mini-CAST provides a dry sample (RH < 40%). The sample was further diluted with filtered and dried air by a dilution factor (DF) of ~ 4 (DF1 in Figure 1) using a simple T-diluter (cylindrical vessel with a diluent inlet on the side) and passed through a cyclone with $1\ \mu\text{m}\ D_{50}$ cutoff diameter, as required in the calibration method to prevent particle shedding from affecting the BC mass instruments (SAE 2013). Afterward, the sample was drawn through the CS at ~ 12 lpm (residence time ~ 2 s). The design specification of the CS (10 lpm flow rate) prevented us from running all the instruments directly after the CS. We therefore used another dilution step with pure (99.999%) nitrogen using a similar diluter by a factor of ~ 8 (DF2 in Figure 1). DF2 was determined by measuring the CO_2 concentrations before and after dilution with two identical CO_2 analyzers (LI-840A; LICOR, Inc., USA). The CO_2 analyzers were calibrated and checked for linearity in the measurement range used (<1% vol.) before and after the campaign. Because the mini-CAST produces low CO_2 concentration (<0.3%), a small amount of CO_2 (<5% by volume after mixing) was mixed into the sample upstream of DF1. DF1 and DF2 were set such that the BC mass instruments reported concentrations $<500\ \mu\text{g}/\text{m}^3$ to mimic values previously measured for in-service aircraft turbine engines with the standardized measurement systems (Lobo et al. 2015). DF2 was used to correct the BC mass data for comparison with the EC/OC filter samples that were taken upstream of DF2 to minimize sampling time.

2.2. EC/OC sampling and analysis

The exhaust sample was drawn through two 47 mm diameter, heat-treated, quartz filters (Pall Tissuequartz; Sigma-Aldrich, LLC; USA) arranged in series and placed in a two-stage stainless steel filter holder (URG-2000-30FXT-QCM; URG Corporation; USA). The flow rate was maintained constant by a mass flow controller (MFC, MKS 1179A; MKS Instruments, USA). We collected 60 filter pairs and sent them to Sunset Laboratory Inc. to be analyzed according to the NIOSH 5040 protocol (NIOSH 2003). Since some OC compounds can pyrolyze and resemble EC, the EC/OC split needs to be corrected by measuring the transmittance of the filter media. Gas phase OC that absorbs on the filter also affects the EC/OC split. We corrected for this artifact by subtracting the OC determined from the secondary filter, which contained almost exclusively adsorbed gas phase OC, from the OC mass determined from the primary filter. The primary filter contained on average $18\ \mu\text{g}/\text{cm}^2$ TC (range: 6–66) and the secondary filter $0.78\ \mu\text{g}/\text{cm}^2$ TC (range: 0.2–1.7).

The EC mass concentrations were calculated from the total sample volume passed through the filter and the EC

mass determined by the thermal-optical analysis. The EC mass deposited on the filter was calculated by multiplying the filter loading area by the EC concentration from the analyzed filter punches ($1\ \text{cm}^2$). The filter EC mass was then divided by the total sample volume passed through the filter calculated from the filter flow rate (at standard temperature and pressure conditions, 0°C and $101.3\ \text{kPa}$) and the sampling time. For each test point, the resulting EC and OC mass concentrations are the average of two to three filter samples. We estimated the errors in the EC mass concentrations and the EC/TC ratios by propagating the measurement uncertainties in the EC and TC mass provided by Sunset Laboratory Inc. and the MFC error (5% at a given flow rate). The relative errors of the EC mass concentration and the EC/TC split ($\pm 1\sigma$) were $8 \pm 0.4\%$ and $8.5 \pm 0.7\%$, respectively.

2.3. Transmission electron microscopy

To investigate the particle morphology and internal structure, particles were collected using an in-house designed axial electrostatic aerosol precipitator (AEAP, Figure 1) on carbon coated copper grids for transmission electron microscopy (TEM) analysis. Representative TEM images for each test point were acquired using an FEI Tecnai F20 operated at 200 kV using a field emission gun high-resolution TEM. Images were taken with the Gatan Ultra Scan CCD with a point resolution of 0.24 nm. At least two areas were imaged at higher magnifications to provide good resolution since both the grid film and particles contained carbon.

2.4. Real-time particle instrumentation

After the last dilution stage, the sample was distributed via a 5-way splitter to the real-time instruments that measured particle number concentration, size distribution, and BC mass concentration (Figure 1). Each instrument was connected to the splitter by a similar length (~ 3 m) of carbon-impregnated conductive silicone tubing. We verified that each instrument received the same sample independent of the position on the splitter by swapping the splitter connections.

The eBC was determined by two MSSs (firmware version 2.05). The MSS measures the eBC mass concentration using the photo-acoustic method. The aerosol is drawn through a temperature-controlled (52°C) open resonant cell where it is exposed to intensity-modulated laser light (near-infrared wavelength $\lambda = 808\ \text{nm}$) at the resonance frequency of the cell ($\sim 4000\ \text{Hz}$). When the light is on, the BC in the soot absorbs the incident light; it heats up, and dissipates the heat to the surrounding gas when the light is off. The periodic warming and cooling of the surrounding gas result in

pressure fluctuations (sound) that are detected by a microphone located in the middle of the cell at the pressure maximum of the standing acoustic wave. The microphone signal is linearly related to BC mass concentration in the measurement volume. The light source wavelength used guarantees negligible interferences from other exhaust components (Schindler et al. 2004). Water and absorbing gases (e.g., NO₂) interfere with the photoacoustic response of soot (Arnott et al. 2003; Lack et al. 2009), but at the wavelength used for a dry (<10% RH) sample they produce negligible BC-equivalent signal (<<1 μg/m³).

The rBC was determined by the LII (firmware version 3.2). The LII measures the rBC mass concentration by absorption of laser radiation, which is transformed into heat and reemitted as thermal radiation (incandescence). The LII uses a Q-switched Nd:YAG laser emitting radiation at 1064 nm at 20 Hz. The particles are heated up to 4000 K, below the sublimation temperature, and the incandescence from the particles is measured by two photomultipliers at 720 nm and 440 nm wavelengths. The measurement cell was heated to 60°C. The incandescence intensity is used to derive number and size of the soot primary particles and thereby the soot volume fraction. LII is insensitive to soot coatings as they evaporate early during the heating without contributing to the incandescence (Slowik et al. 2007).

The MSSs and LII were independently calibrated using different soot sources. Each instrument was run in parallel with an EC/OC sampling system. The correlation coefficients were determined from linear regressions of the instrument signals and the EC mass determined by the NIOSH 5040 method (NIOSH 2003). EC was determined from at least four filters spanning the concentration range from 50 μg/m³ to 1000 μg/m³. The MSSs were calibrated by the manufacturer AVL using a propane-fueled CAST aerosol generator. The LII was fluence-optimized (i.e., finding the pulse energy that gives the highest incandescence) and calibrated in the laboratories of the National Research Council Canada using a methane-fueled inverted flame burner. Both the calibration sources produced ≥80% EC, but optical properties, such as the mass-specific absorption cross-section (MAC, m²/g), are unknown. The accuracy of this calibration is expected to be within ±10%, reflecting the limitations of the calibration method, reference material, and inter-laboratory variability (SAE 2013).

Particle size distributions in mobility equivalent diameter, d_m , were measured using the fast particle spectrometer DMS500 (Cambustion, Ltd., UK; Biskos et al. 2005). The DMS500 has been widely used in studies that characterized aircraft turbine engine emissions (Lobo et al. 2012; Lobo et al. 2015). Prior to measurement by the DMS500, the exhaust sample was diluted once more

with a HEPA filter dilution bridge (dilution factor ~2) to prevent fouling of the classifier and its frequent cleaning.

The nvPM number concentration was measured by an AVL Particle Counter Advanced (APC; AVL LIST GmbH, Austria). The APC consists of a two-stage rotating disc diluter (dilution factor maintained at ~176 for this study), a catalytic stripper (350°C), and a condensation particle counter (CPC; Model 3790E, TSI, Inc., Shoreview, MN, USA) with a 10 nm D₅₀ cutoff diameter. This instrument was only used to monitor particle number concentration and the stability of the mini-CAST since it is more sensitive than the BC mass instruments and is less affected by particle properties.

2.5. Effective density and primary particle size

Particle effective density was determined from tandem aerosol classification by particle mobility and mass. The mini-CAST aerosol was first classified by an in-house designed DMA (column length = 72.8 cm, outer cylinder ID = 8.89 cm, inner rod OD = 5.08 cm). This DMA was previously used in numerous lab and field studies (Schmid et al. 2002, and references therein). The sample and sheath flow rates were 3 lpm and 20 lpm, respectively. The DMA-classified aerosol was drawn through the centrifugal particle mass analyzer (CPMA; Cambustion, Ltd., UK) that classifies particles by their mass/charge ratio between two concentrically spinning cylinders with an electric field between them (Olfert and Collings 2005). The DMA-CPMA classified particles were counted by a CPC (Model 3775, TSI, Inc., USA, D₅₀ = 4 nm). The CPMA was operated in the scanning mode by stepping the angular velocity and voltage while keeping the DMA settings constant.

Prior to the mini-CAST experiments, we verified the DMA-CPMA performance using NaCl aerosol. The particle mass, m_p , obtained for a given DMA-selected d_m was used to calculate the d_m using material density of 2160 kg/m³ and the dynamic shape factor of 1.08 (Kelly and McMurry 1992). The calculated d_m agreed with the DMA-selected value on average within 2.5% (range 0.5%–6.8%) in the 25–200 nm range.

The m_p was determined as the mode of a log-normal distribution fitted to the DMA-CPMA output function. This mode gives the average mass of singly charged particles. However, for loose soot agglomerates, the DMA-CPMA may not completely separate singly charged particles (Olfert et al. 2007). When multiply charged particles are present, the output function distribution is positively skewed (Radney and Zangmeister 2015). Since the distributions were symmetric, we did

not consider multiply charged particles to affect the determined m_p and effective density.

The particle effective density was calculated as $\rho_{\text{eff}} = 6m_p / \pi d_m^3$. Since soot particles are fractal-like agglomerates, their morphology can be approximated by scaling laws (Sorensen 2011). The effective density distribution of fractal-like agglomerates follows a power-law relationship:

$$\rho_{\text{eff}} = A d_m^{D_{\text{fm}} - 3}, \quad [1]$$

where A is the mass-mobility pre-factor and D_{fm} is the mass-mobility exponent.

Effective density distributions were used to estimate the primary particle diameters, d_{pp} , using the theory of Diffusion Limited Cluster Aggregation (DLCA; Jullien et al. 1987; Sorensen 2011). According to the DLCA theory, soot aggregates typically have fractal dimension of 1.8 and their mobility diameters scale with the number and size of primary particles. The effective density of DLCA agglomerates that have less than 100 primary particles can be estimated from the d_{pp} , d_m , and the material density, ρ_M , as Equation (S26) in the supplementary information of Mamakos et al. (2013):

$$\rho_{\text{eff}} = \rho_M \left(\frac{d_m}{d_{\text{pp}}} \right)^{2.17-3}. \quad [2]$$

Similar to Mamakos et al. (2013), we fitted Equation (2) to the experimentally determined effective densities to find d_{pp} that best represents the experimental data. Instead of

using a constant material density of 2000 kg/m^3 , we calculated the material density from the EC/OC data. We assumed densities of 1800 kg/m^3 and 1300 kg/m^3 for EC and OC, respectively, according to Adler et al. (2010), and references therein.

2.6. Variability and reproducibility

The same flow conditions for two mini-CAST burners of the same model may produce soot with different EC content, d_g , and concentration. The same is true for repeated measurements of one burner over long periods. Previously, one burner tested over a period of several months reproduced the d_g and particle number concentrations within 20% and 50%, respectively (Moore et al. 2014). To minimize the intra-day variability, test matrices for each burner were executed within three consecutive days. Within this short period, d_g and effective density distributions of duplicate measurements at one burner setting varied within 10%. While the variability plays an important role for characterization of the operating conditions (see the SI), we primarily investigate the response of the BC instruments with respect to the measured properties rather than the specific flow settings.

3. Results and discussion

3.1. Effect of EC/TC

The eBC (measured by the MSS) and rBC (measured by the LII) agreed with the thermal-optical EC to various extents as a function of the EC/TC and the mini-CAST

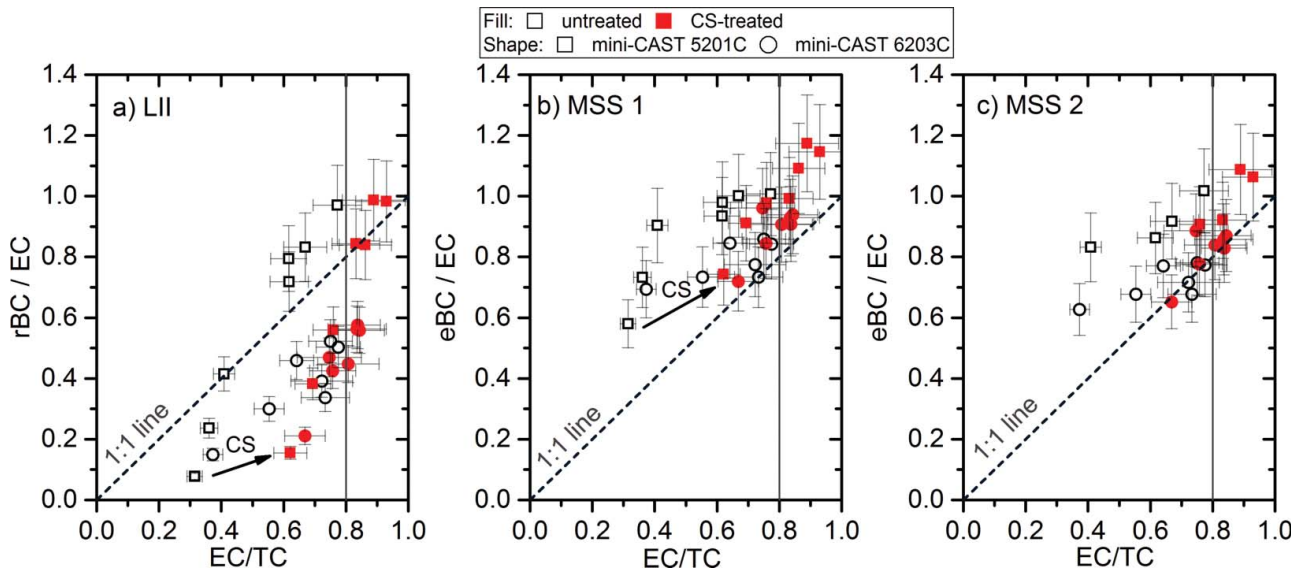


Figure 2. Ratios of the real-time BC to filter EC as a function of the EC/TC for the LII (a), MSS 1 (b), and MSS 2 (c). Error bars represent the propagated errors in the BC and EC mass concentrations. We assumed 10% error for BC mass concentration measurement and the average error in the EC mass concentration was 8%. MSS 2 data were not logged at all test conditions.

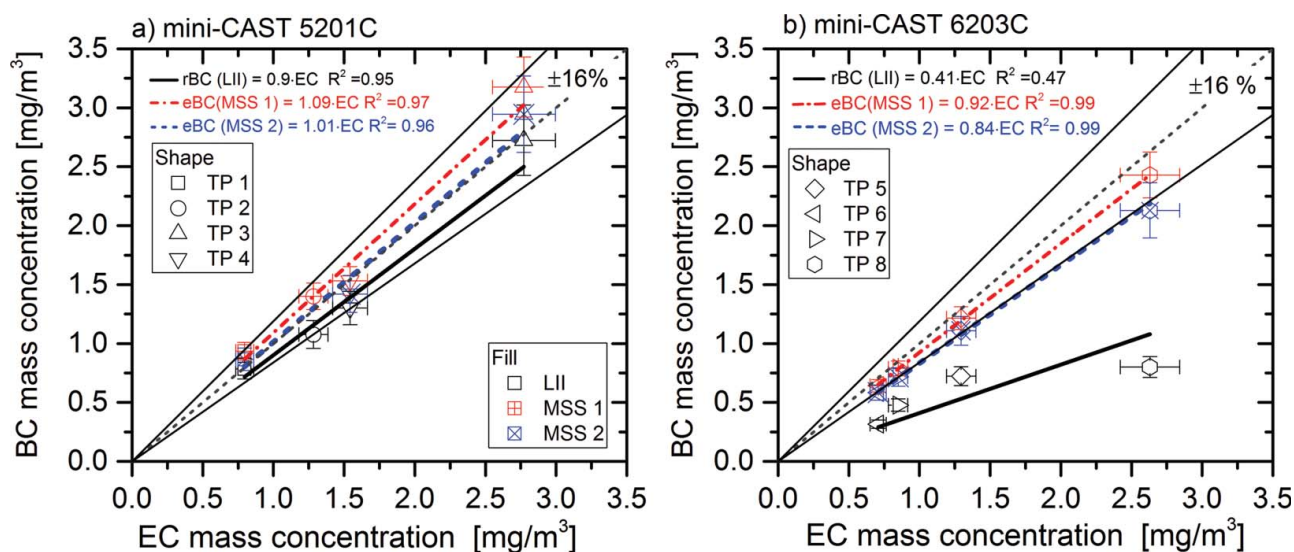
Table 1. Summary of the mini-CAST settings, EC/TC, d_g , and d_{pp} for the eight selected test points with the highest EC/TC using the CS.

Test point	Source	Q_f [mlpm]	$Q_{mix\ N_2}$ [mlpm]	Q_a [lpm]	Q_{N_2} [lpm]	Q_{dil} [lpm]	ϕ	C:O	EC/TC	d_g [nm]	d_{pp} [nm]	D_{fm}
1	5201C	60	0	1.7	7	20	0.86	0.26	0.89	152	26	2.13
2	5201C	60	100	1.7	7	20	0.86	0.26	0.86	98	17	2.16
3	5201C	60	0	1.45	7	20	1.01	0.30	0.93	161	45	2.19
4	5201C	60	200	1.45	7	20	1.01	0.30	0.83	85	23	2.11
5	6203C	20	0	1	1	10	0.49	0.15	0.84	72	15	2.15
6	6203C	20	5	1	1	10	0.49	0.15	0.81	55	15	2.14
7	6203C	15	0	0.6	1	10	0.61	0.18	0.84	74	15	2.11
8	6203C	25	0	0.8	1	10	0.76	0.23	0.84	58	25	2.23

model (Figure 2). As EC/TC decreased, both the eBC and rBC underreported the EC, but the rBC diverged more severely (Figure 2a). At the lowest EC/TC (0.31), the rBC/EC and eBC/EC reached 7% and 58%, respectively, and increased after treating the sample by the CS. After the CS treatment, the EC/TC doubled (0.62; details in Table S1 in the SI) and the rBC/EC and eBC/EC reached 15% and 75%, respectively (marked by arrows in Figures 2a and b). For the mini-CAST 5201C, the rBC/EC shows an almost linear dependence on EC/TC for both the untreated and CS-treated soot (Figure 2a). The eBC/EC shows a similar trend for the CS-treated soot, whereas the untreated samples appear to be independent of EC/TC for EC/TC > ~0.4 (Figures 2b and c). For the samples with EC/TC > 0.8, the eBC overreported the EC while the rBC/EC remained close to unity. Both the MSS and LII responded differently to mini-CAST 6203C soot. The rBC/EC and eBC/EC were lower than the mini-CAST 5201C samples at similar EC/TC. Even for EC/TC > 0.8, the rBC/EC reached only 58% whereas the eBC/EC reached 93%.

The BC-EC discrepancy is linked to changing light absorption properties with soot structure (Bond and Bergstrom 2006). With decreasing EC/TC, the primary soot particles became less distinguishable and the internal structure less graphitized (TEM images in Table S4 in the SI). The heat treatment by the CS partially removed the semi-volatile OC and improved graphitization. The OC in mini-CAST soot, rather than being a transparent non-absorbing soot coating, is a “weakly” absorbing semi-volatile and non-volatile “brown” carbon that can be efficiently removed only at ~500°C (Mamakos et al. 2013). Light absorption of mini-CAST soot OC strongly depends on wavelength (Kim et al. 2015). The differences could be seen on the filter samples, where the EC-rich samples were black and the OC-rich were brown.

The spectral dependence of OC absorption may be linked to the differences between eBC and rBC at OC-rich conditions. The relative absorption function of the LII (function of the complex refractive index) decreases and becomes strongly wavelength dependent as particles

**Figure 3.** Comparison of the real-time BC (DF 2 corrected) with the filter EC for EC/TC > 0.8 for test points 1–4 generated by the mini-CAST 5201C (a) and test points 5–8 generated by the mini-CAST 6203C (b).

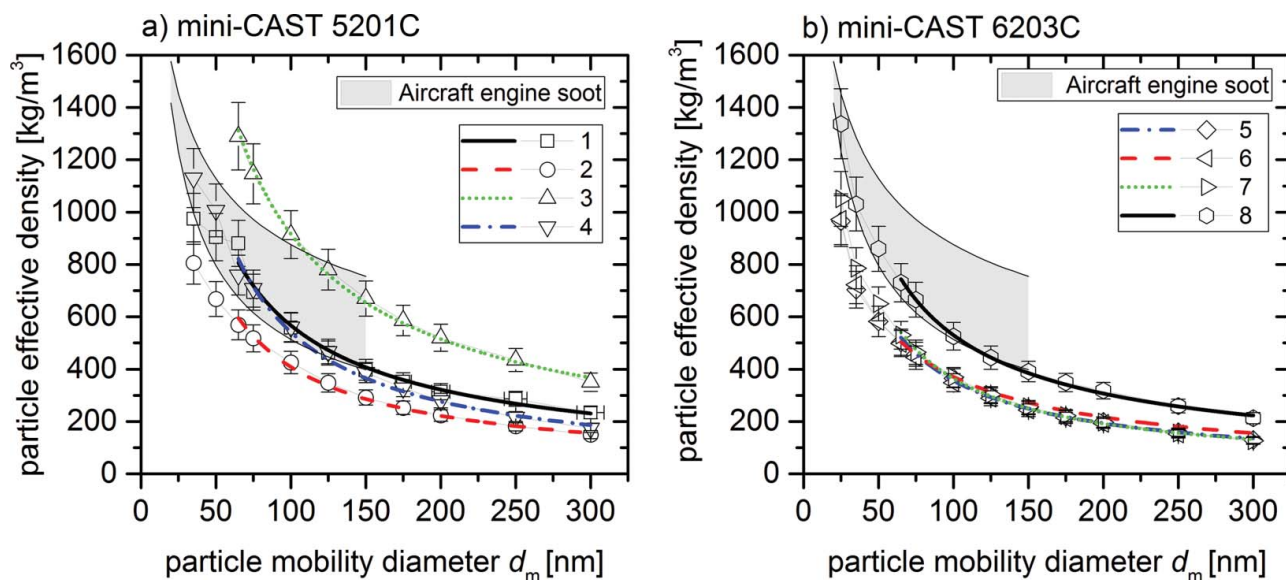


Figure 4. Effective density distributions for test points 1–4 generated by the mini-CAST 5201C (a) and test points 5–8 generated by the mini-CAST 6203C (b). Error bars represent the assumed errors of 10% for effective density and 3% for particle size measurement. The gray areas show the range of effective density distributions found for aircraft turbine engines using the same technique (Durdina et al. 2014; Lobo et al. 2015).

become less mature with liquid-like structure, similar to the OC-rich conditions in this study (Table S4 in the SI). Such particles require higher laser fluence to incandesce than mature soot (Olofsson et al. 2013). However, even for the most mature soot with EC/TC > 0.8, the rBC/EC varied twice as much as the eBC/EC (Figure 2). Since these conditions would qualify as calibration aerosols for nvPM mass concentration measurements, we limit our further observations to a subset of conditions summarized in Table 1.

Four test points were chosen for each mini-CAST, spanning from fuel-lean to stoichiometric and treated by the CS (Figure 3). For both the mini-CASTs, eBC agreed well with EC ($R^2 > 0.95$, slopes within 16% of the 1:1 line). However, rBC agreed well only for test points 1–4 ($R^2 = 0.95$, slope 0.9). The rBC-EC agreement was rather poor for test points 5–8 ($R^2 = 0.41$, slope 0.47). This striking difference suggests that properties other than EC/TC may affect the instruments response.

3.2. Effect of particle morphology and size

Effective density decreased with particle mobility size for all the test points, following a power-law relationship (Figure 4). The lines in Figure 4 represent the power-law fits of Equation (1) (fitted particle size range from 65 nm to 300 nm). The error bars represent the uncertainties for the DMA classification (3%; Kinney et al. 1991) and the effective density determined by the DMA-CPMA system (10%; Johnson et al. 2013). The mass-mobility exponents, D_{fm} , were similar for all test points (~ 2.15 ;

Table 1). The D_{fm} determined is similar to previous mini-CAST and diesel soot studies (Mamakos et al. 2013; Maricq 2014; Moore et al. 2014), but is lower than D_{fm} of aircraft turbine engine soot determined with the same method (~ 2.35 – 2.65 , Durdina et al. 2014; Lobo et al. 2015). This suggests that mini-CAST soot is less compact than aircraft engine soot. The different D_{fm} of these soot types should not affect the BC measurements, because soot MAC is independent of D_{fm} (Radney et al. 2014). While the D_{fm} was similar for all the test points, the effective density strongly varied for a given particle size. For example, effective density of 100 nm mobility diameter particle at test point 3 was more than factor of 2 higher than at test point 2 (Figure 4a). Overall, effective density increased with ϕ and decreased with N_2 premix (Table S3 in the SI).

Effective density increased with increasing primary particle size, similar to previous findings (Mamakos et al. 2013). The estimated primary particle size from DMA-CPMA measurements and DLCA theory (Equation (2)) ranged from 15 nm to 43 nm (Table 1). We also observed such differences in primary particle size in the TEM images that agree relatively well with the estimates (Figure 5).

Test points 1, 4, and 8 produced soot with effective densities closest to aircraft gas turbine soot. The gray areas in Figure 4 represent the range of effective density distributions found for in-service aircraft turbofan engines with different combustors and running at various power levels (Durdina et al. 2014; Lobo et al. 2015). The estimated d_{pp} for these points are similar to a turbofan engine at high power (Liatl et al. 2014; Vander Wal et al. 2014), however these mini-CAST settings produced

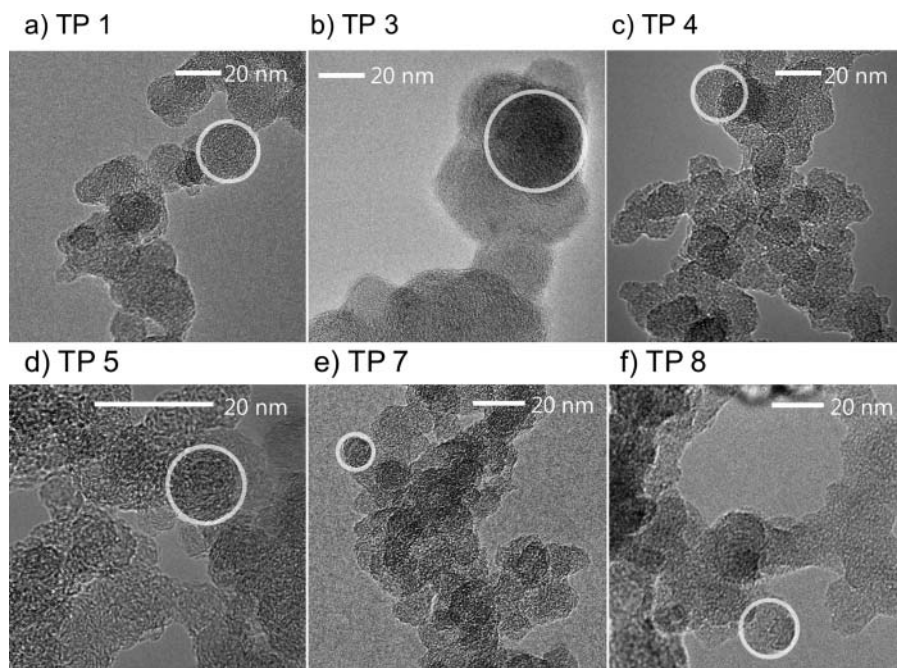


Figure 5. TEM images of soot particles. Circles represent the estimated primary particle diameter from DMA-CPMA measurements and the DLCA theory.

a wide range of d_g that were larger than observed in the aircraft engine exhaust (Figure 6a).

The different relative response of the MSS and LII seems to be linked to soot agglomerate size and is roughly independent of primary particle size (Figure 6). This can be seen, *e.g.*, on test points 1, 4, and 8 that produced similar d_{pp} (~ 25 nm), but different d_g (58 nm–152 nm; Figure 6a). The rBC/EC and eBC/EC for these

points were independent of d_{pp} (Figure 6b), but the difference between rBC/EC and eBC/EC increased with decreasing d_g (Figure 6c). A similar trend can be observed for test points 2, 5, 6, and 7 that produced d_{pp} of ~ 15 nm and d_g ranging from 55 nm to 100 nm. Over the eight test points, the difference between rBC and eBC increased (relative to MSS 1 data) from 15% at ~ 160 nm to 50% at ~ 50 nm.

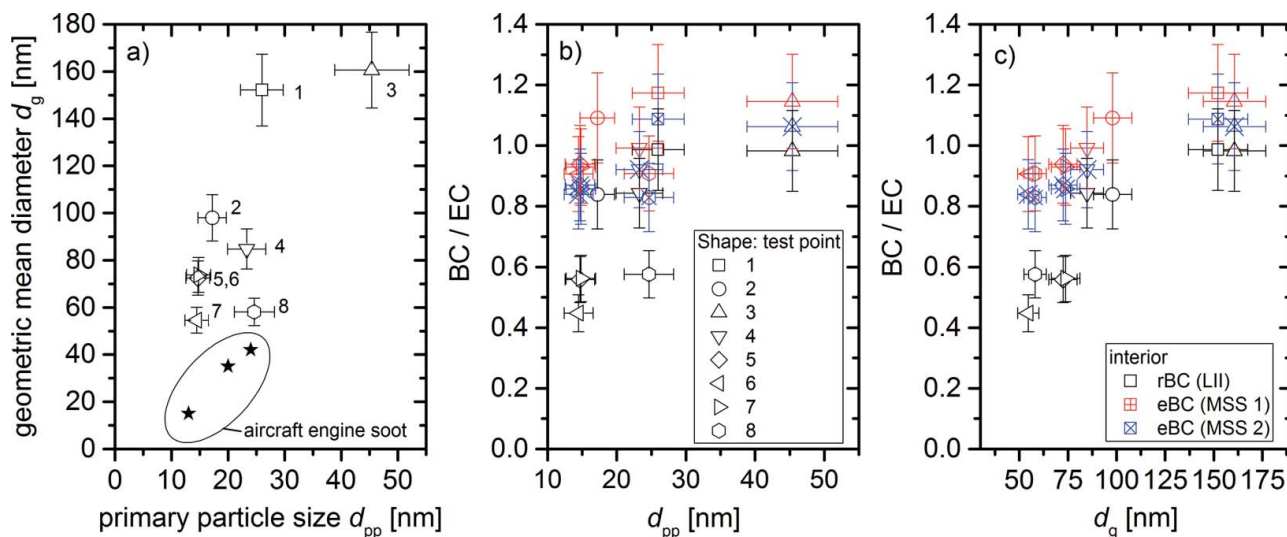


Figure 6. Geometric mean diameter as a function of primary particle size compared for mini-CAST test points 1–8 and aircraft engine soot (Durdina et al. 2014; Liati et al. 2014) (a); BC/EC response as a function of the primary particle size (b) and the geometric mean diameter (c).

The effect of soot agglomerate size on the LII response is thought to be independent of EC mass concentration. For example, test points 3 and 8 produced similar EC mass concentrations (Figure 3), but the rBC was $\sim 30\%$ lower at test point 8 that generated smaller agglomerates (Figure 6). The MSS and LII have been found to respond linearly ($R^2 > 0.99$) as a function of soot mass concentration on a fixed mini-CAST setting with different dilution ratios except for reported concentrations below $< 5 \mu\text{g}/\text{m}^3$ (Lobo et al. 2015). Here, the MSS and LII reported at least 67 and $30 \mu\text{g}/\text{m}^3$, respectively.

While it is unclear how these differences would translate to real-world combustion engine soot measurements, the LII sensitivity to agglomerate size may explain the differences observed in aircraft turbine engine measurements (Durdina et al. 2014). At the ambient conditions and the instrument settings used, the LII response is expected to be independent of agglomerate size and morphology. The agglomerate size affects the signal only at high pressure and high laser fluence (pulse energy per area) and is unimportant at atmospheric pressure and low fluence as used here (Bladh et al. 2008; Liu and Smallwood 2011).

Since the laser fluence was optimized for the calibration aerosol, it may not be optimal for other sources. Both high and low laser fluence levels can underestimate the soot volume fraction. Higher laser fluence is required to incandesce loose soot agglomerates with small primary particles ($d_{\text{pp}} < 10 \text{ nm}$ and $D_{\text{fm}} = 2$) because of their larger surface area (Gysel et al. 2012). On the other hand, too high laser fluence can vaporize the soot to certain depth, leaving less material to incandesce. Although the LII was operated at low fluence levels $\sim 0.15 \text{ J}/\text{cm}^2$, below the often used threshold for soot vaporization of $0.2 \text{ J}/\text{cm}^2$, fluence should be below $0.1 \text{ J}/\text{cm}^2$ to eliminate the possibility of any soot vaporization (Yoder et al. 2005). Therefore, this effect cannot be completely excluded.

4. Conclusions

The plethora of definitions of soot and soot surrogates based on optical properties or chemical compositions makes it challenging to specify a surrogate aerosol for real-world emissions, being ideally an inexpensive material that could be used for calibration of various instruments. The real-time BC instruments used for regulatory measurements of nvPM mass-based emissions from aircraft turbine engines are referenced to EC determined by a thermal-optical method using diffusion flame soot that contains $\geq 80\%$ EC. This loose criterion may not guarantee acceptable performance during actual aircraft turbine engine measurements. Therefore, the performance of real-time BC instruments needs to

be assessed on gas turbine soot as well as using potential calibration sources.

We have shown that two real-time BC instruments, the MSS and LII, respond differently to mini-CAST soot with various compositions and morphologies. We used two mini-CAST burners to produce soot with a wide range of EC/TC ratios, effective densities, and d_g by changing ϕ , pre-mixing N_2 into the fuel, and switching between the CS-treated and untreated sample. The soot properties varied not only with flame conditions but also with the burner design. As EC/TC decreased, the rBC (LII) and eBC (MSS) underreported the EC. The LII was shown to be much more susceptible to underestimating the EC mass concentration at low EC/TC, moreover, the rBC/EC varied by up to 60% at conditions with EC/TC > 0.8 .

For the eight selected test points with EC/TC > 0.8 , we found the MSS to agree better with EC (within $\pm 16\%$) suggesting that the MSS may be more robust and less sensitive to calibration aerosol properties other than EC/TC. Both the MSS and LII responded independently of primary particle size, but the LII seemed to be affected by the geometric mean size of the soot agglomerates. The rBC/EC ratio steeply decreased with decreasing d_g . We therefore suggest taking the particle size distributions of the calibration aerosol into account.

If mini-CAST soot is to be used for calibrating the instruments measuring nvPM mass concentrations, setting the conditions by ϕ might produce completely different d_g and EC/TC for various burner models. Since EC content of mini-CAST soot decreases with decreasing d_g , generating soot with high EC content, and a small agglomerate size ($d_g < 50 \text{ nm}$) typical for aircraft gas turbines seem to be conflicting requirements. Therefore, other sources should be investigated. These findings may contribute to improving the specifications for the calibration method for nvPM mass concentration measurements in the exhaust of aircraft turbine engines and may also apply to regulatory measurements of other soot sources.

Acknowledgments

The authors thank Dr. Clarissa Wisner of Materials Research Center at Missouri S&T for the TEM images.

Funding

This study was funded and supported by the Center of Excellence for Aerospace Particulate Emissions Reduction Research at Missouri University of Science and Technology (Missouri S&T) and the Swiss Federal Office for Civil Aviation project "Particulate Matter and Gas Phase Emission Measurement of Aircraft Engine Exhaust."

References

- Adler, G., Riziq, A. A., Erlick, C., and Rudich, Y. (2010). Effect of Intrinsic Organic Carbon on The Optical Properties of Fresh Diesel Soot. *P. Natl. A. Sci.*, 107:6699–6704.
- Agrawal, H., Sawant, A. A., Jansen, K., Wayne Miller, J., and Cocker, D. R. (2008). Characterization of Chemical and Particulate Emissions from Aircraft Engines. *Atmos. Environ.*, 42:4380–4392.
- Arnott, W. P., Moosmüller, H., Sheridan, P. J., Ogren, J. A., Raspert, R., Slaton, W. V., Hand, J. L., Kreidenweis, S. M., and Collett, J. L. (2003). Photoacoustic and Filter-Based Ambient Aerosol Light Absorption Measurements. Instrument Comparisons and The role of Relative Humidity. *J. Geophys. Res.*, 108:AAC 15-1–AAC 15-11.
- Attfield, M. D., Schleiff, P. L., Lubin, J. H., Blair, A., Stewart, P. A., Vermeulen, R., Coble, J. B., and Silverman, D. T. (2012). The Diesel Exhaust in Miners Study. A Cohort Mortality Study With Emphasis on Lung Cancer. *J. Natl. Cancer. I.*, 104:869–883.
- Baumgardner, D., Popovicheva, O., Allan, J., Bernardoni, V., Cao, J., Cavalli, F., Cozic, J., Diapouli, E., Eleftheriadis, K., Genberg, P. J., Gonzalez, C., Gysel, M., John, A., Kirchstetter, T. W., Kuhlbusch, T. A. J., Laborde, M., Lack, D., Müller, T., Niessner, R., Petzold, A., Piazzalunga, A., Putaud, J. P., Schwarz, J., Sheridan, P., Subramanian, R., Swietlicki, E., Valli, G., Vecchi, R., and Viana, M. (2012). Soot Reference Materials for Instrument Calibration and Intercomparisons. A Workshop Summary With Recommendations. *Atmos. Meas. Tech.*, 5:1869–1887.
- Birch, M. E., and Cary, R. A. (1996). Elemental Carbon-Based Method for Monitoring Occupational Exposures to Particulate Diesel Exhaust. *Aerosol Sci. Technol.*, 25:221–241.
- Biskos, G., Reavell, K., and Collings, N. (2005). Description and Theoretical Analysis of a Differential Mobility Spectrometer. *Aerosol Sci. Technol.*, 39:527–541.
- Bladh, H., Johnsson, J., and Bengtsson, P.-E. (2008). On the Dependence of the Laser-Induced Incandescence (LII) Signal on Soot Volume Fraction for Variations in Particle Size. *Appl. Phys. B*, 90:109–125.
- Bond, T. C., and Bergstrom, R. W. (2006). Light Absorption by Carbonaceous Particles. An Investigative Review. *Aerosol Sci. Technol.*, 40:27–67.
- Bond, T. C., Doherty, S. J., Fahey, D. W., Forster, P. M., Berntsen, T., DeAngelo, B. J., Flanner, M. G., Ghan, S., Kärcher, B., Koch, D., Kinne, S., Kondo, Y., Quinn, P. K., Sarofim, M. C., Schultz, M. G., Schulz, M., Venkataraman, C., Zhang, H., Zhang, S., Bellouin, N., Guttikunda, S. K., Hopke, P. K., Jacobson, M. Z., Kaiser, J. W., Klimont, Z., Lohmann, U., Schwarz, J. P., Shindell, D., Storelvmo, T., Warren, S. G., and Zender, C. S. (2013). Bounding the Role of Black Carbon in the Climate System. A Scientific Assessment. *J. Geophys. Res.-Atmos.*, 118:5380–5552.
- Crayford, A., Johnson, M., Llamedo, A., Williams, P., Madden, P., Marsh, R., and Bowen, P. (2013). *Studying, Sampling and Measuring of Aircraft Particulate Emissions III - Specific Contract 03: SAMPLE III - SC.03*. European Aviation Safety Agency, Cologne, Germany.
- Cross, E. S., Onasch, T. B., Ahern, A., Wrobel, W., Slowik, J. G., Olfert, J., Lack, D. A., Massoli, P., Cappa, C. D., Schwarz, J. P., Spackman, J. R., Fahey, D. W., Sedlacek, A., Trimborn, A., Jayne, J. T., Freedman, A., Williams, L. R., Ng, N. L., Mazzoleni, C., Dubey, M., Brem, B., Kok, G., Subramanian, R., Freitag, S., Clarke, A., Thornhill, D., Marr, L. C., Kolb, C. E., Worsnop, D. R., and Davidovits, P. (2010). Soot Particle Studies—Instrument Inter-Comparison—Project Overview. *Aerosol Sci. Technol.*, 44:592–611.
- DieselNet (2016). Emission Standards. Summary of Worldwide Engine Emission Standards. Available at: <https://www.dieselnet.com/standards/>.
- Durdina, L., Brem, B. T., Abegglen, M., Lobo, P., Rindlisbacher, T., Thomson, K. A., Smallwood, G. J., Hagen, D. E., Sierau, B., and Wang, J. (2014). Determination of PM Mass Emissions From An Aircraft Turbine Engine using Particle Effective Density. *Atmos. Environ.*, 99:500–507.
- Giechaskiel, B., Maricq, M., Ntziachristos, L., Dardiotis, C., Wang, X., Axmann, H., Bergmann, A., and Schindler, W. (2014). Review of Motor Vehicle Particulate Emissions Sampling and Measurement. From Smoke and Filter Mass to Particle Number. *J. Aerosol Sci.*, 67:48–86.
- Gysel, M., Laborde, M., Corbin, J. C., Mensah, A. A., Keller, A., Kim, J., Petzold, A., and Sierau, B. (2012). Technical Note. The single Particle Soot Photometer Fails to Detect PALAS Soot Nanoparticles. *Atmos. Meas. Tech. Discuss.*, 5:4905–4925.
- Jacobson, M. Z. (2001). Strong Radiative Heating Due to the Mixing State of Black Carbon in Atmospheric Aerosols. *Nature*, 409:695–697.
- Jing, L. (2002). Influence of Air on the Soot Particles in Co-Flow Diffusion Flame. Available at: http://www.sootgenerator.com/documents/jing_b.pdf.
- Johnson, T. J., Symonds, J. P. R., and Olfert, J. S. (2013). Mass-Mobility Measurements Using a Centrifugal Particle Mass Analyzer and Differential Mobility Spectrometer. *Aerosol Sci. Technol.*, 47:1215–1225.
- Jullien, R., Botet, R., and Mors, P. M. (1987). Computer Simulations of Cluster-Cluster Aggregation. *Faraday Discuss. Chem. Soc.*, 83:125–137.
- Kelly, W. P., and McMurry, P. H. (1992). Measurement of Particle Density by Inertial Classification of Differential Mobility Analyzer-Generated Monodisperse Aerosols. *Aerosol Sci. Technol.*, 17:199–212.
- Kim, J., Bauer, H., Dobovičnik, T., Hitzenberger, R., Lottin, D., Ferry, D., and Petzold, A. (2015). Assessing Optical Properties and Refractive Index of Combustion Aerosol Particles Through Combined Experimental and Modeling Studies. *Aerosol Sci. Technol.*, 49:340–350.
- Kinney, P. D., Pui, D., Mulholland, G. W., and Bryner, N. P. (1991). Use of the Electrostatic Classification Method to size 0.1 Micrometer SRM Particles - A Feasibility Study. *J. Res. Nat. Inst. Stan.*, 96:147–176.
- Lack, D. A., Cappa, C. D., Covert, D. S., Baynard, T., Massoli, P., Sierau, B., Bates, T. S., Quinn, P. K., Lovejoy, E. R., and Ravishankara, A. R. (2008). Bias in Filter-Based Aerosol Light Absorption Measurements Due to Organic Aerosol Loading. Evidence from Ambient Measurements. *Aerosol Sci. Technol.*, 42:1033–1041.
- Lack, D. A., Cappa, C. D., Cross, E. S., Massoli, P., Ahern, A. T., Davidovits, P., and Onasch, T. B. (2009). Absorption Enhancement of Coated Absorbing Aerosols. Validation of the Photo-Acoustic Technique for Measuring the Enhancement. *Aerosol Sci. Technol.*, 43:1006–1012.
- Lack, D. A., and Corbett, J. J. (2012). Black Carbon From Ships. A Review of the Effects of Ship Speed, Fuel Quality and Exhaust Gas Scrubbing. *Atmos. Chem. Phys.*, 12:3985–4000.

- Lack, D. A., Moosmüller, H., McMeeking, G. R., Chakrabarty, R. K., and Baumgardner, D. (2014). Characterizing Elemental, Equivalent Black, and Refractory Black Carbon Aerosol Particles: A Review of Techniques, Their Limitations and Uncertainties. *Anal. Bioanal. Chem.*, 406:99–122.
- Liat, A., Brem, B. T., Durdina, L., Vöggtli, M., Dasilva, Y. A. R., Eggenschwiler, P. D., and Wang, J. (2014). Electron Microscopic Study of Soot Particulate Matter Emissions From Aircraft Turbine Engines. *Environ. Sci. Technol.*, 48:10975–10983.
- Liscinsky, D. S., Yu, Z., True, B., Peck, J., Jennings, A. C., Wong, H.-W., Franklin, J., Herndon, S. C., and Miake-Lye, R. C. (2013). Measurement of Naphthalene Uptake by Combustion Soot Particles. *Environ. Sci. Technol.*, 47:4875–4881.
- Liu, F., and Smallwood, G. J. (2011). The Effect of Particle Aggregation on the Absorption and Emission Properties of Mono- and Polydisperse Soot Aggregates. *Appl. Phys. B*, 104:343–355.
- Lobo, P., Durdina, L., Smallwood, G. J., Rindlisbacher, T., Siegerist, F., Black, E. A., Yu, Z., Mensah, A. A., Hagen, D. E., Miake-Lye, R. C., Thomson, K. A., Brem, B. T., Corbin, J. C., Abegglen, M., Sierau, B., Whitefield, P. D., and Wang, J. (2015). Measurement of Aircraft Engine Non-Volatile PM Emissions. Results of the Aviation-Particle Regulatory Instrumentation Demonstration Experiment (A-PRIDE) 4 Campaign. *Aerosol Sci. Technol.*, 49:472–484.
- Lobo, P., Hagen, D. E., and Whitefield, P. D. (2012). Measurement and Analysis of Aircraft Engine PM Emissions Downwind of an Active Runway at the Oakland International Airport. *Atmos. Environ.*, 61:114–123.
- Mamakos, A., Khalek, I., Giannelli, R., and Spears, M. (2013). Characterization of Combustion Aerosol Produced by a Mini-CAST and Treated in a Catalytic Stripper. *Aerosol Sci. Technol.*, 47:927–936.
- Maricq, M. M. (2014). Examining the Relationship Between Black Carbon and Soot in Flames and Engine Exhaust. *Aerosol Sci. Technol.*, 48:620–629.
- Menon, S., Hansen, J., Nazarenko, L., and Luo, Y. (2002). Climate Effects of Black Carbon Aerosols in China and India. *Science*, 297:2250–2253.
- Mohr, M., Lehmann, U., and Rütter, J. (2005). Comparison of Mass-Based and Non-Mass-Based Particle Measurement Systems for Ultra-Low Emissions from Automotive Sources. *Environ. Sci. Technol.*, 39:2229–2238.
- Moore, R. H., Ziemba, L. D., Dutcher, D. D., Beyersdorf, A. J., Chan, K., Crumeyrolle, S. N., Raymond, T. M., Thornhill, K. L., Winstead, E. L., and Anderson, B. E. (2014). Mapping the Operation of the Miniature Combustion Aerosol Standard (Mini-CAST) Soot Generator. *Aerosol Sci. Technol.*, 48:467–479.
- NIOSH (2003). *Method 5040, Issue 3 (Interim): Elemental Carbon (Diesel Exhaust) in NIOSH Manual of Analytical Methods*. National Institute of Occupational Safety and Health, Cincinnati, OH.
- Oberdorster, G., Sharp, Z., Atudorei, V., Elder, A., Gelein, R., Kreyling, W., and Cox, C. (2004). Translocation of Inhaled Ultrafine Particles to the Brain. *Inhal. Toxicol.*, 16:437–445.
- Olfert, J. S., and Collings, N. (2005). New Method for Particle Mass Classification—the Couette Centrifugal Particle Mass Analyzer. *J. Aerosol Sci.*, 36:1338–1352.
- Olfert, J. S., Symonds, J., and Collings, N. (2007). The Effective Density and Fractal Dimension of Particles Emitted From a Light-Duty Diesel Vehicle With a Diesel Oxidation Catalyst. *J. Aerosol Sci.*, 38:69–82.
- Olofsson, N.-E., Johnsson, J., Bladh, H., and Bengtsson, P.-E. (2013). Soot Sublimation Studies in a Premixed Flat Flame Using Laser-Induced Incandescence (LII) and Elastic Light Scattering (ELS). *Appl. Phys. B*, 112:333–342.
- Ostro, B., Hu, J., Goldberg, D., Reynolds, P., Hertz, A., Bernstein, L., and Kleeman, M. J. (2015). Associations of Mortality With Long-Term Exposures to Fine and Ultrafine Particles, Species and Sources: Results From the California Teachers Study Cohort. *Environ. Health Persp.*, 123:549–556.
- Petzold, A., Marsh, R., Johnson, M., Miller, M., Sevcenco, Y., Delhaye, D., Ibrahim, A., Williams, P., Bauer, H., Crayford, A., Bachalo, W. D., and Raper, D. (2011). Evaluation of Methods for Measuring Particulate Matter Emissions from Gas Turbines. *Environ. Sci. Technol.*, 45:3562–3568.
- Petzold, A., Ogren, J. A., Fiebig, M., Laj, P., Li, S.-M., Baltensperger, U., Holzer-Popp, T., Kinne, S., Pappalardo, G., Sugimoto, N., Wehrli, C., Wiedensohler, A., and Zhang, X.-Y. (2013). Recommendations for Reporting “Black Carbon” Measurements. *Atmos. Chem. Phys.*, 13:8365–8379.
- Pöschl, U. (2005). Atmospheric Aerosols. Composition, Transformation, Climate and Health Effects. *Angew. Chem. Int. Ed.*, 44:7520–7540.
- Radney, J. G., You, R., Ma, X., Conny, J. M., Zachariah, M. R., Hodges, J. T., and Zangmeister, C. D. (2014). Dependence of Soot Optical Properties on Particle Morphology: Measurements and Model Comparisons. *Environ. Sci. Technol.*, 48:3169–3176.
- Radney, J. G., and Zangmeister, C. D. (2015). Practical Limitations of Aerosol Separation by a Tandem Differential Mobility Analyzer–Aerosol Particle Mass Analyzer. *Aerosol Sci. Technol.*, 50:160–172.
- Ramanathan, V., and Carmichael, G. (2008). Global and Regional Climate Changes due to Black Carbon. *Nat. Geosci.*, 1:221–227.
- Ristovski, Z. D., Miljevic, B., Surawski, N. C., Morawska, L., Fong, K. M., Goh, F., and Yang, I. A. (2012). Respiratory Health Effects of Diesel Particulate Matter. *Respirol. (Carlton, Vic.)*, 17:201–212.
- Saathoff, H., Naumann, K.-H., Schnaiter, M., Schöck, W., Weingartner, E., Baltensperger, U., Krämer, L., Bozoki, Z., Pöschl, U., Niessner, R., and Schurath, U. (2003). Carbon Mass Determinations During the AIDA Soot Aerosol Campaign 1999. *J. Aerosol Sci.*, 34:1399–1420.
- SAE (2013). *Aerospace Information Report (AIR) 6241. Procedure for the Continuous Sampling and Measurement of Non-Volatile Particle Emissions from Aircraft Turbine Engines*. SAE International, Warrendale, PA.
- Schindler, W., Haisch, C., Beck, H. A., Niessner, R., Jacob, E., and Rothe, D. (2004). *A Photoacoustic Sensor System for Time Resolved Quantification of Diesel Soot Emissions*. SAE Technical Paper 2004-01-0968. SAE International, Warrendale, PA.
- Schmid, O., Trueblood, M. B., Gregg, N., Hagen, D. E., and Whitefield, P. D. (2002). Sizing of Aerosol in Gases Other Than Air Using a Differential Mobility Analyzer. *Aerosol Sci. Technol.*, 36:351–360.

- Schnaiter, M., Gimmler, M., Llamas, I., Linke, C., Jäger, C., and Mutschke, H. (2006). Strong Spectral Dependence of Light Absorption by Organic Carbon Particles Formed by Propane Combustion. *Atmos. Chem. Phys. Discuss.*, 6:1841–1866.
- Sheridan, P. J., Arnott, W. P., Ogren, J. A., Andrews, E., Atkinson, D. B., Covert, D. S., Moosmüller, H., Petzold, A., Schmid, B., Strawa, A. W., Varma, R., and Virkkula, A. (2005). The Reno Aerosol Optics Study. An Evaluation of Aerosol Absorption Measurement Methods. *Aerosol Sci. Technol.*, 39:1–16.
- Slowik, J. G., Cross, E. S., Han, J.-H., Davidovits, P., Onasch, T. B., Jayne, J. T., Williams, L. R., Canagaratna, M. R., Worsnop, D. R., Chakrabarty, R. K., Moosmüller, H., Arnott, W. P., Schwarz, J. P., Gao, R.-S., Fahey, D. W., Kok, G. L., and Petzold, A. (2007). An Inter-Comparison of Instruments Measuring Black Carbon Content of Soot Particles. *Aerosol Sci. Technol.*, 41:295–314.
- Sorensen, C. M. (2011). The Mobility of Fractal Aggregates. A Review. *Aerosol Sci. Technol.*, 45:765–779.
- Stettler, M. E. J., Swanson, J. J., Barrett, S. R. H., and Boies, A. M. (2013). Updated Correlation Between Aircraft Smoke Number and Black Carbon Concentration. *Aerosol Sci. Technol.*, 47:1205–1214.
- Subramanian, R., Roden, C. A., Boparai, P., and Bond, T. C. (2007). Yellow Beads and Missing Particles. Trouble Ahead for Filter-Based Absorption Measurements. *Aerosol Sci. Technol.*, 41:630–637.
- Vander Wal, R. L., Bryg, V. M., and Huang, C.-H. (2014). Aircraft Engine Particulate Matter. Macro- micro- and Nanostructure by HRTEM and Chemistry by XPS. *Combust. Flame*, 161:602–611.
- Wong, H.-W., Beyersdorf, A. J., Heath, C. M., Ziemba, L. D., Winstead, E. L., Thornhill, K. L., Tacina, K. M., Ross, R. C., Albo, S. E., Bulzan, D. L., Anderson, B. E., and Miake-Lye, R. C. (2013). Laboratory and Modeling Studies on the Effects of Water and Soot Emissions and Ambient Conditions on the Properties of Contrail ice Particles in the Jet Regime. *Atmos. Chem. Phys.*, 13:10049–10060.
- Yoder, G. D., Diwakar, P. K., and Hahn, D. W. (2005). Assessment of Soot Particle Vaporization Effects During Laser-Induced Incandescence With Time-Resolved Light Scattering. *Appl. Opt.*, 44:4211–4219.